*Article*

# Facile Synthesis of Poly(*o*-anisidine)/Graphitic Carbon Nitride/Zinc Oxide Composite for Photo-Catalytic Degradation of Congo Red Dye

Mohammed Jalalah [1,2], Zubair Nabi [3], Muhammad Naveed Anjum [3,*], Mirza Nadeem Ahmad [3], Atta Ul Haq [4], Muhammad Bilal Qadir [5,*], Mohd Faisal [1,6], Mabkhoot Alsaiari [1,7], Muhammad Irfan [2] and Farid A. Harraz [1,7,*]

[1] Promising Centre for Sensors and Electronic Devices (PCSED), Advanced Materials and Nano-Research Centre, Najran University, Najran 11001, Saudi Arabia
[2] Electrical Engineering Department, College of Engineering, Najran University, Najran 61441, Saudi Arabia
[3] Department of Applied Chemistry, Government College University, Faisalabad 38000, Pakistan
[4] Department of Chemistry, Government College University Faisalabad 38000, Pakistan
[5] Department of Textile Engineering, National Textile University, Faisalabad 37610, Pakistan
[6] Department of Chemistry, Faculty of Science and Arts, Najran University, Najran 11001, Saudi Arabia
[7] Department of Chemistry, Faculty of Science and Arts at Sharurah, Najran University, Sharurah 68342, Saudi Arabia
* Correspondence: anjumccj@hotmail.com (M.N.A.); bilal_ntu81@hotmail.com (M.B.Q.); faharraz@nu.edu.sa (F.A.H.)

**Abstract:** Growing industry and its effluents create a serious environmental concern. Various industrial wastes such as toxic dyes and volatile organic compounds are posing a threat to a clean environment because of their non-biodegradable nature and high chemical stability. In recent years, the degradation of toxic dyes and drugs by photo-catalysts has gained much importance and proved a successful approach to capture light by hybrid photo-catalysts for decomposing toxic organic molecules. This work presents the synthesis of a poly(*o*-anisidine)-based composite with graphitic carbon nitride and zinc oxide (POA/g-C$_3$N$_4$/ZnO) and its utilization as a photo-catalyst. Various analytical techniques investigated the synthesized photo-catalysts' chemical structure, crystallinity, and morphology. The degradation of Congo red dye evaluated the efficiency of the photo-catalyst in an aqueous medium under ultraviolet light. It was revealed that the photo-catalytic activity of the synthesized POA/g-C$_3$N$_4$/ZnO composites show 81.43%, 92.28%, and 87.05% degradation. This sustainable composite will be highly beneficial to treat industrial wastewater to make our environment clean.

**Keywords:** poly(*o*-anisidine); graphitic carbon nitride; zinc oxide; ternary composite; photo-catalytic degradation; Congo red; industrial wastewater treatment

## 1. Introduction

Water is a basic need for all living things, used for drinking, washing, agriculture, and other purposes. These days, the scarcity of drinking water and the importance of water have become a major concern for researchers due to changes occurring in climate. Water pollution is increasing significantly with the advent of chemical industry and the concomitant growing population. Industrial and agricultural wastewater and domestic sewage are the major causes of water pollution [1]. Among these wastes, industrial wastewater involves organic and inorganic elements which include chemical dyes, pesticide residues, fertilizers, volatile organic compounds, and detergents. Various toxic dyes, drugs, and volatile organic compounds are of much concern because of their stable chemistry and non-biodegradable nature [2]. The industrial processes of dyeing cloth, paper and pulp manufacturing, leather

treatment, food, medicine, cosmetics, and plastics, use synthetic organic dyes, and about 17–20% of water pollution has been caused by industrial effluents [3].

Different methods are employed to eliminate dyes from wastewater. These methods are electrodialysis [4], chemical treatment [5], adsorption [6], membrane separation process [7], conventional coagulation [8], and photo-catalytic degradation [9]. Keeping the efficiency of these methods in view, photo-catalytic degradation is widely used because of its high efficiency in organic degradation and its cost-effective technology [10].

In recent years, conductive polymeric materials having conjugated bonds has gained the attention of scientists and engineers. Polyaniline, polypyrrole, and poly(*o*-anisidine) are conducting polymers that have been widely used in scientific and industrial research, as well as in various applications, e.g., rechargeable batteries, sensors, and diodes, as well as transistors and microelectronic devices. For example, Manea et al. have developed mesoporous Sm@POA/TP and POA/TP nanocomposites to enhance the performance of the photo-catalytic degradation of MB and MG dyes [11]. Poly(*o*-anisidine) has gotten a lot of interest among these conducting polymers because of its excellent ecological stability, good electrical conductivity, and easy synthesis [12].

In 1996, Teter and Hemley published the first study on $C_3N_4$, resulting in five molecular structures: $\alpha$-$C_3N_4$, $\beta$-$C_3N_4$, g-$C_3N_4$, p-$C_3N_4$, and c-$C_3N_4$. Among them, g-$C_3N_4$ is the most stable and has the lowest density at normal conditions [13,14]. The concentration of carbon and nitrogen in g-$C_3N_4$ enhances the accepter/donor properties, which improves the active reaction sites and wettability with electrolytes. The photo-catalyst g-$C_3N_4$ is used for various photo-redox processes, including artificial photosynthesis, environmental cleanup, pollutant degradation, and bacterial disinfection. To improve its photo-catalytic efficacy, it is typically doped with other elements, co-polymerized with other substances, or mixed with semiconductors and metals [15,16]. Paul et al. have reported zinc carbonate basic dihydrate and urea-derived g-$C_3N_4$−ZnO composites result in better photo-catalytic ability toward degradation of the Methylene blue (MB) dye [17].

ZnO is an n-type semiconductor with a varied range of band gaps ($E_g$ = 3.37) and a wide range of excitation binding energy (60 meV) [18]. As compared to other metal oxide semiconductors, zinc oxide is the most often used photo-catalyst for the detoxification of inorganic and organic compounds. It has excellent multi-disciplinary properties, e.g., high activity and photosensitivity, good chemical stability, low cost, chemical and physical stability, easy synthesis, non-toxicity, excellent photo-catalytic activity, and biocompatibility [19,20]. It shows poor light absorption properties because it can absorb only ultraviolet light with a wavelength shorter than 387 nm. Furthermore, the photo-catalytic activity of zinc oxide is also reduced as a result of the quick recombination of photo-generated $e^-/h^+$ pairs. Therefore, poor light absorption and low charge separation decrease the usage of zinc oxide at a large scale [21]. Mohd et al. fabricated the novel metal-organic framework ZIF-8 with poly(*o*-anisidine)/zinc oxide to synthesize non-hybrid PAZ@ZIF-8 material. AZ@ZIF-8 has shown high removal effectiveness towards the removal of Malachite Green (MG) dye, and approximately 96% of the dye is removed within a very short amount of time, as compared to ZIF-8 (34%) and POA/ZnO (61%) [22].

## 2. Results and Discussion

Given all the above, we combined POA with g-$C_3N_4$ and ZnO to prepare a POA/g-$C_3N_4$/ZnO composite photo-catalyst by chemical oxidative polymerization technique. Herein, we report the design of a photo-catalytic system that photo-degrades the organic pollutants by using POA/g-$C_3N_4$/ZnO as composite catalysts. The current work not only offers a perfect example of how photo-degradation can function, but it also creates a brand-new path toward removing organic contaminants from wastewater [23]. The synthesized poly(*o*-anisidine)/graphitic carbon nitride/zinc oxide composite was characterized by using FTIR (Spectrum 2, Perkin Elmer, Waltham, MA, USA), XRD (D8 Advance Bruker, Vancouver, BC, Canada and SEM (Cube II EmCrafts, Gyeonggi, Republic of Korea). Fourier transform infrared spectroscopy (FTIR) analyzed the functional groups of the composites.

The composite crystallinity was examined by X-ray diffraction (XRD). Finally, the morphology and composite electrode homogeneous dispersion were indicated by scanning electron microscopy (SEM).

*2.1. X-ray Diffraction (XRD)*

The crystalline structure of ZnO, g-C$_3$N$_4$, S1, S2, and S3 of POA/g-C$_3$N$_4$/ZnO composites with different polymer ratios were characterized by using XRD, which are shown in Figure 1. The XRD peaks of the pure ZnO NPs are quite comparable to the hexagonal wurtzite crystal phase of ZnO (JCPDS 65-3411) [24]. The XRD characteristic curve of pure g-C$_3$N$_4$ shows a significant peak at 2θ = 27.17° which is related to the inter-layer structural packing motif and the typical inter-layer stacking of the conjugated aromatic CN units (JCPDS 87-1526) [25]. Due to interactions between g-C$_3$N$_4$ and ZnO NPs, the main peaks exhibit a minor shift toward a higher Bragg's angle, which identifies the contraction and expansion of the lattice of ZnO respectively [26]. Additionally, a characteristic peak for g-C$_3$N$_4$ that initially emerged at 27.17° and was later moved to 27.66° provided improved indication when combined with POA and ZnO NPs. In POA/g-C$_3$N$_4$/ZnO composites, the distinctive ZnO peaks completely vanished which may be due to doping of the ZnO in POA/g-C$_3$N$_4$/ZnO composite. However, POA shows no broad peak which is due to the amorphous nature of the material. Additionally, the coexistence of POA, g-C$_3$N$_4$, and ZnO diffraction planes in all composites' XRD patterns indicate that the three materials were successfully composited [27].
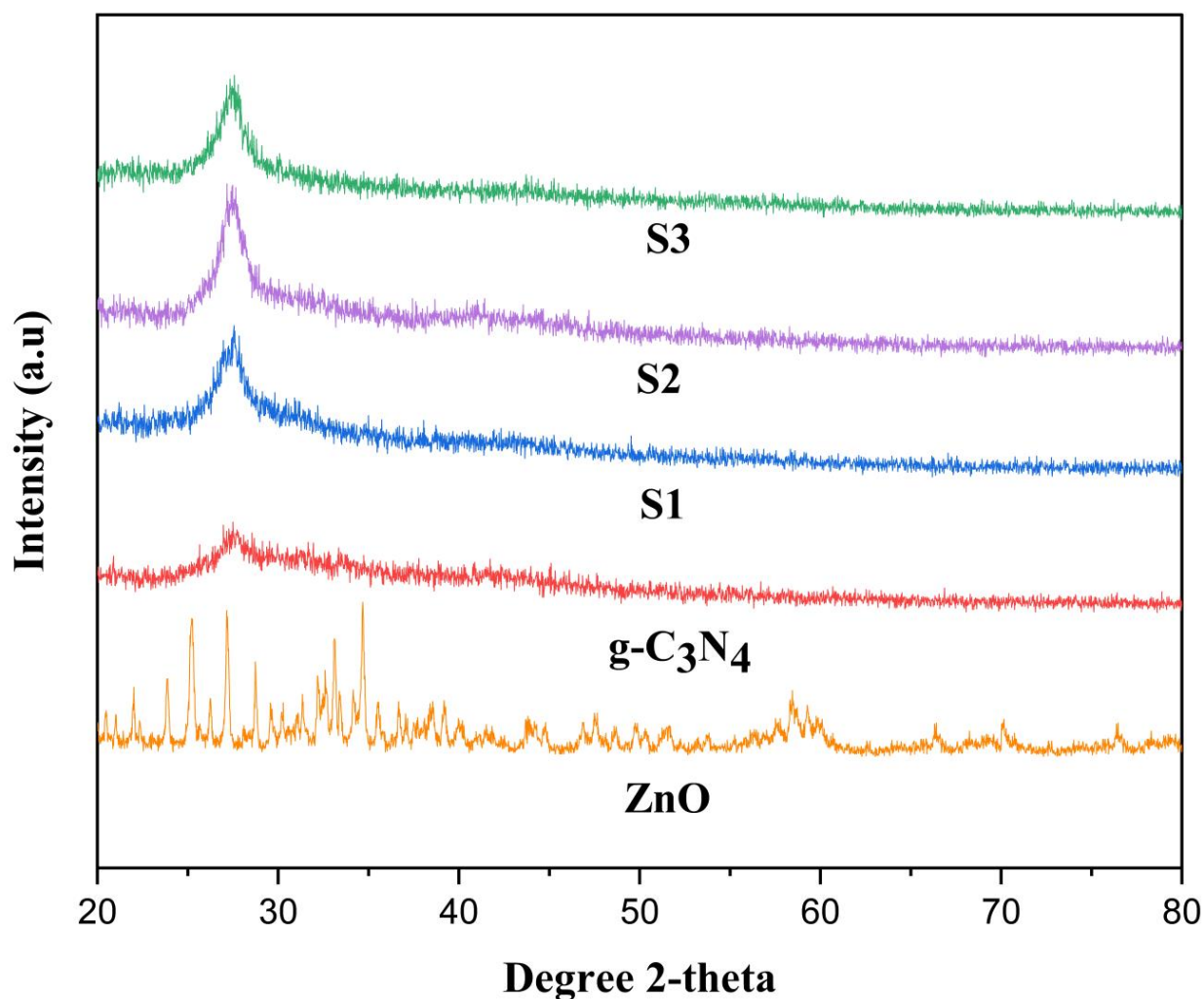


**Figure 1.** XRD of ZnO, g-C$_3$N$_4$, S1, S2, and S3 POA/g-C$_3$N$_4$/ZnO composites.

## 2.2. Fourier Transform Infrared Spectroscopy (FTIR)

FT-IR spectroscopy is used to identify the chemical structure of the pure g-$C_3N_4$ and generated POA/g-$C_3N_4$/ZnO composite photo-catalyst [28]. As seen in Figure 2, pure g-$C_3N_4$ exhibits that the C=N stretching vibration mode is responsible for the peak at 1533 cm$^{-1}$, while aromatic C-N stretching is responsible for the peaks at 1237, 1398, and 1637 cm$^{-1}$, respectively. The s-triazine ring's distinctive breathing pattern is related to the peak at 806 cm$^{-1}$. The primary and secondary amines' stretching modes and their interactions within the molecules of other molecules can be attributed to the peak ranging from 2900 to 3400 cm$^{-1}$ region [29]. In the IR spectra, 1553 and 1489 cm$^{-1}$ are established by C=C stretching vibrations of the quinoid and rings, respectively [11]. The distinctive absorption band of the POA/g-$C_3N_4$/ZnO composites are similar to those of the bulk material, demonstrating that thermal exfoliation did not affect the chemical composition of the g-$C_3N_4$ network [30]. Poor crystallinity observed for POA/g-$C_3N_4$/ZnO composites that may cause more defects related to the g-$C_3N_4$ phase. Such a condition might play a vital role in promoting its activity as a photo-catalyst [17].
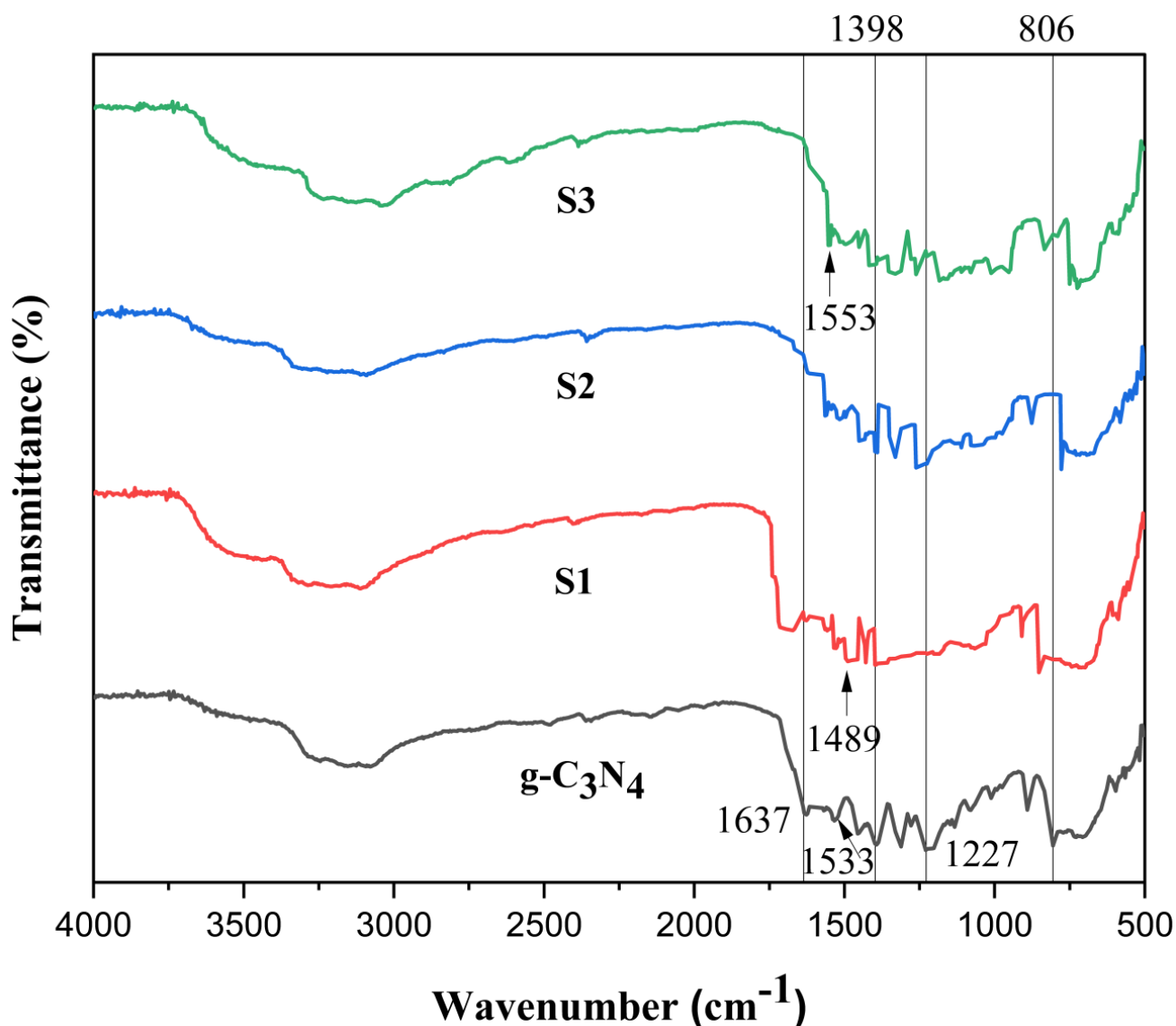


**Figure 2.** FTIR of g-$C_3N_4$, S1, S2, and S3 POA/g-$C_3N_4$/ZnO composites.

### 2.3. Scanning Electron Microscope (SEM)

The morphology of the synthesized POA/g-C$_3$N$_4$/ZnO composites is shown in Figure 3. The SEM images reveal an irregularly shaped structure and demonstrate various tightly or loosely aggregated sheets in various sizes. Due to in situ polymerization on g-C$_3$N$_4$, the POA is assembled on the material's surface and displays a sheet-like shape. Furthermore, it can be observed that ZnO nanostructures are encapsulated in carbon nitride sheets, producing the networks between the g-C$_3$N$_4$ sheets. The POA/g-C$_3$N$_4$/ZnO composites exhibit sponge-like porous structures composed of many nanoparticles, dissimilar from the morphology of pure POA/g-C$_3$N$_4$ and ZnO. The results confirmed the synthesis of POA/g-C$_3$N$_4$/ZnO composites [31].
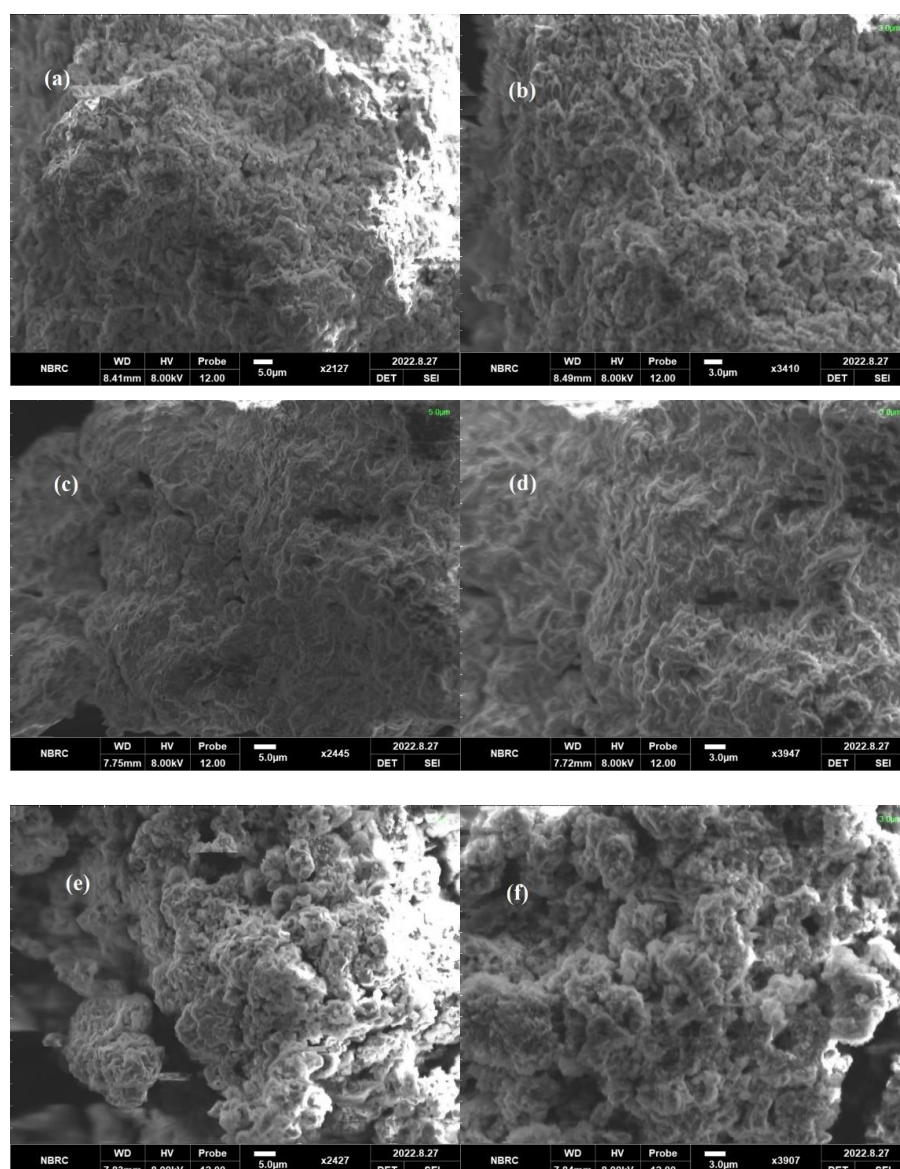


**Figure 3.** SEM of (**a**,**b**) S1, (**c**,**d**) S2, and (**e**,**f**) S3 POA/g-C$_3$N$_4$/ZnO composites.

### 2.4. Photo-Catalytic Activity

The photo-catalytic properties of ZnO NPs, g-C$_3$N$_4$, and POA/g-C$_3$N$_4$/ZnO composites were estimated by the degradation of Congo red (CR) dye in an aqueous medium under UV light. The degradation ratio of CR under various conditions is shown in Figure 4, where C represents the concentration of CR just after irradiation and Co represents the CR concentration following 60 min of adsorption in complete darkness. Throughout 2 h, ZnO

NPs showed 18.30%, and g-$C_3N_4$ showed 36.60% degradation of CR, shown in Figure 4. The degradation rate of ZnO NPs was lower compared to g-$C_3N_4$ due to the poor absorption ability of UV light which was unable to create sufficient $e^-$ and $h^+$ for the degradation of dye [32]. However, g-$C_3N_4$ showed good absorption ability under UV light; as a result, it created sufficient $e^-$ and $h^+$ for the degradation of CR dye. The degradation rates of S1, S2, and S3 POA/g-$C_3N_4$/ZnO composites were around 81.43%, 92.28%, and 87.05%, shown in Figure 4. Although adding POA is favorable to enhancing the charge transfer rate for the degradation of dye, excess POA would lead to a decrease in the degradation rate [33]. Therefore, POA/g-$C_3N_4$/ZnO composites' photo-catalytic activity decreased when the POA content was increased to 2 mL. The POA/g-$C_3N_4$/ZnO composites have a much higher binding affinity for CR molecules than pristine g-$C_3N_4$ and ZnO because it is a hybrid and contains several functional groups from g-$C_3N_4$, ZnO, and POA. In the initial stage, the CR molecules in solution quickly interact with the active site of the POA/g-$C_3N_4$/ZnO composite. In the second stage, the CR molecules that had been adsorbed were degraded through photo-catalysis. The results revealed that the POA/g-$C_3N_4$/ZnO composite decomposed CR molecules more effectively than pure g-$C_3N_4$ and ZnO due to improved $e^-/h^+$ pair separation and lower bandgap energy. The results demonstrate that the POA/g-$C_3N_4$/ZnO composite is effective for CR molecule degradation.



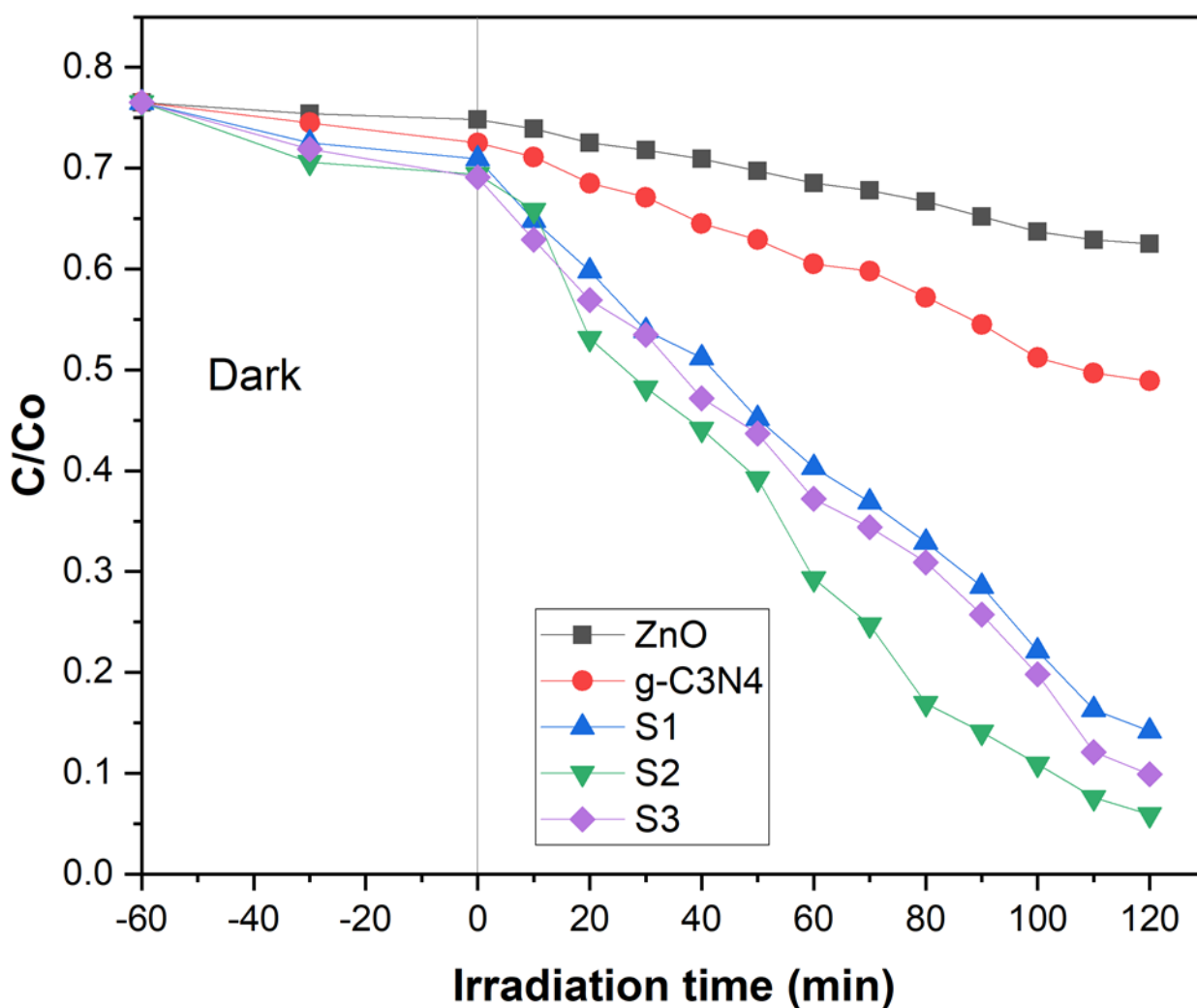**Figure 4.** Photo-catalysis of ZnO, g-$C_3N_4$, and S1, S2, and S3 POA/g-$C_3N_4$/ZnO composites on Congo red dye.

### 2.4.1. pH Effect on CR Dye Degradation

The pH and concentration of dye greatly influence photo-catalysis. Therefore, the pH adjustment is essential for the total photo-catalytic degradation of dyes. In addition, pH affects the catalyst surface ionization state; therefore, finding optimal pH is difficult. Using an optimized CR dye concentration and catalyst quantity, the reaction mixture pH was changed from 2.00 to 10.04 to determine the ideal pH for the degradation of CR dye. The addition of diluted HCl and NaOH solutions changed the pH. The CR dye solution pH was normally 7. The study showed that the CR dye degradation percentage increased from 92.3% to 96% when the solution pH was lowered from 7 to 2.

Additionally, raising the solution pH from 7 to 10 reduced the CR dye photo-degradation to 59% from 92.3%. Owing to CR dye's anionic nature and the presence of two sulphonic groups, the catalyst performs better at low pH for CR dye degradation [34]. These groups are quickly ionized in an acidic environment and produce a soluble CR anion. Additionally, at lower pH levels, more protons are available to protonate the hydroxyl groups in POA/g-$C_3N_4$/ZnO composites and create an electrostatic attraction that will draw a certain amount of dye anion into the material. Because of the positive surface charges of POA/g-$C_3N_4$/ZnO composites, CR anions were readily adsorbed to them at low pH levels. However, at higher pH levels, more negatively charged sites on the adsorbent prevented CR anions from adhering to the catalyst's surface. Due to electrostatic repulsion, an anionic dye cannot be adsorbed to a negatively charged spot on the adsorbent [35]. The results conclude that the acidic medium favors the degradation of CR dye compared to the basic medium, as shown in Figure 5.
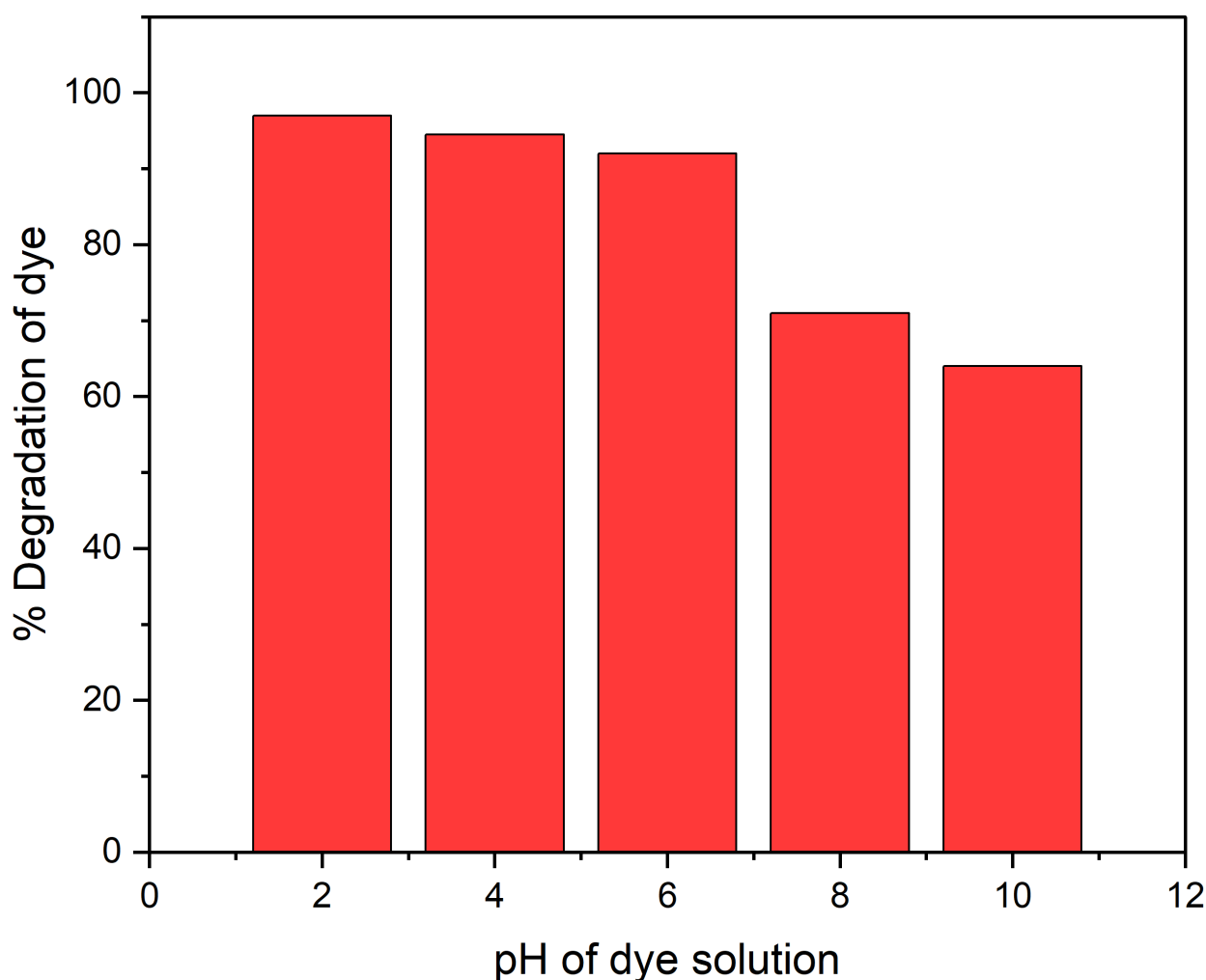


**Figure 5.** pH effect on CR dye degradation under UV light.

### 2.4.2. Effect of Dye Concentration

The CR dye concentration effect on photo-degradation was investigated with differing concentrations within a 10–50 ppm range with a fixed amount of catalyst. The result showed that 96% photo-catalytic degradation of CR was obtained at 10 ppm dye concentration. However, as the concentration of dye increased to 50 ppm, the degradation decreased to 68%, as shown in Figure 6. This may be explained by the fact that as dye concentration increases, the amount of light that reaches the photo-catalyst surface decreases; as a result, it generates less photo-generated reactive radicals, which causes a drop in photo-catalytic activity at higher initial dye concentration [36].
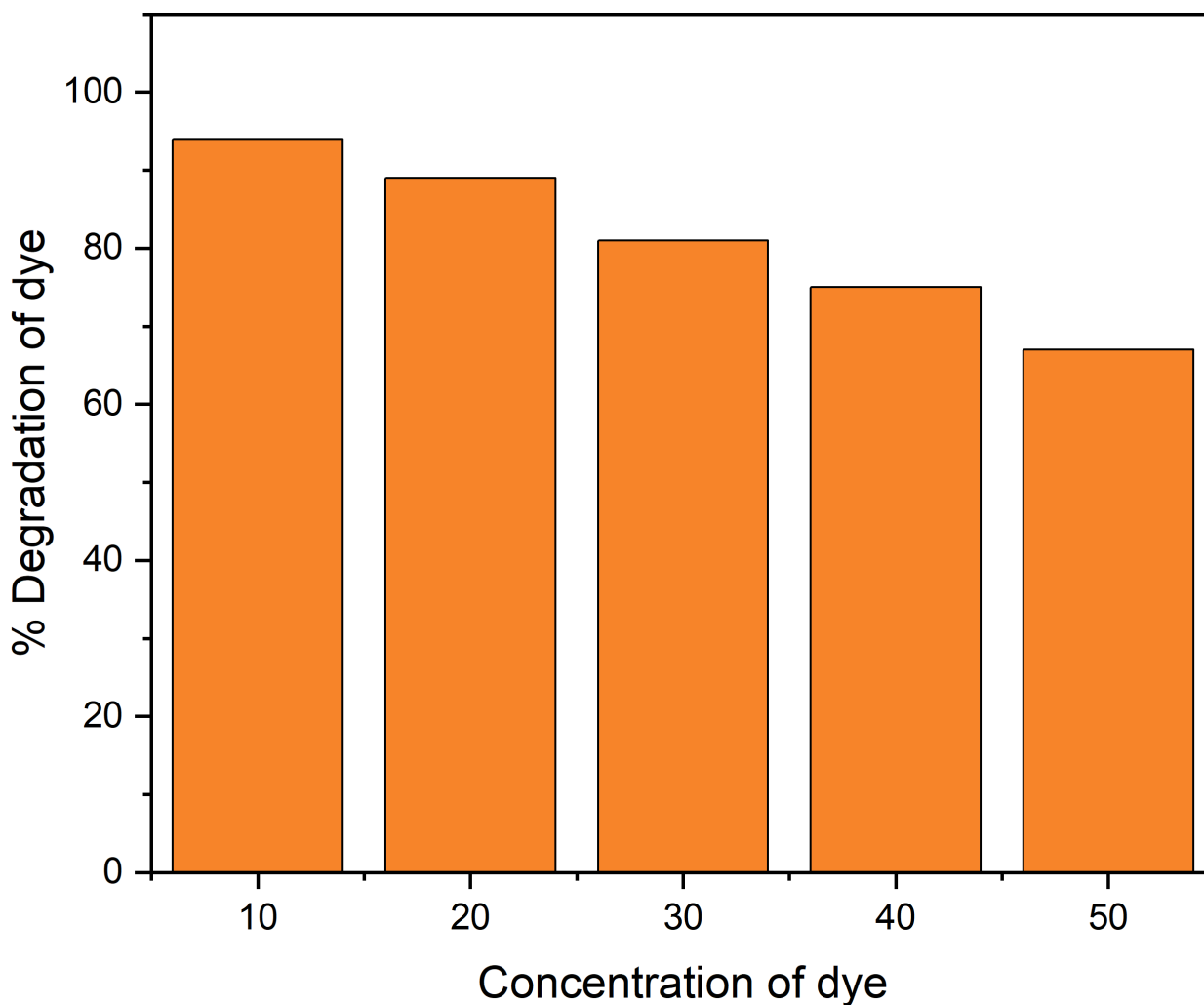


**Figure 6.** Dye concentration effect for the degradation of CR dye under UV light.

### 2.4.3. Kinetic Analysis

Kinetic analysis is an essential factor in determining the reaction route. Various researchers have proved that the Langmuir–Hinshelwood kinetic expression is compatible with the pseudo-first-order kinetic model for heterogeneous photo-catalysis [37,38]. Therefore, the Langmuir–Hinshelwood model can be written as shown in Equation (1):

$$r = kKC_t/1 + KC_t \approx k_{app}C_t \tag{1}$$

$K$ is the reactant adsorption constant, $k_{app}$ is the reaction rate constant, and $C_t$ is the dye concentration at time $t$. Also, Equation (1) can be summarized by integration:

$$\ln(C_0/C) = kt \tag{2}$$

$C_0$ is the dye solution starting concentration, and $k$ is a rate constant. It is demonstrated in Figure 7 by the straight line on the plot of $\ln C_0/C$ vs. irradiation time $t$ that the degradation of CR dye observes the pseudo-first-order kinetics. Additionally, the L–H kinetic model for the CR dye photo-degradation was validated by the regression coefficient ($R^2$) of 0.973, which is close to 1 and indicates that the photo-catalyst follows the pseudo-first-order kinetic model.
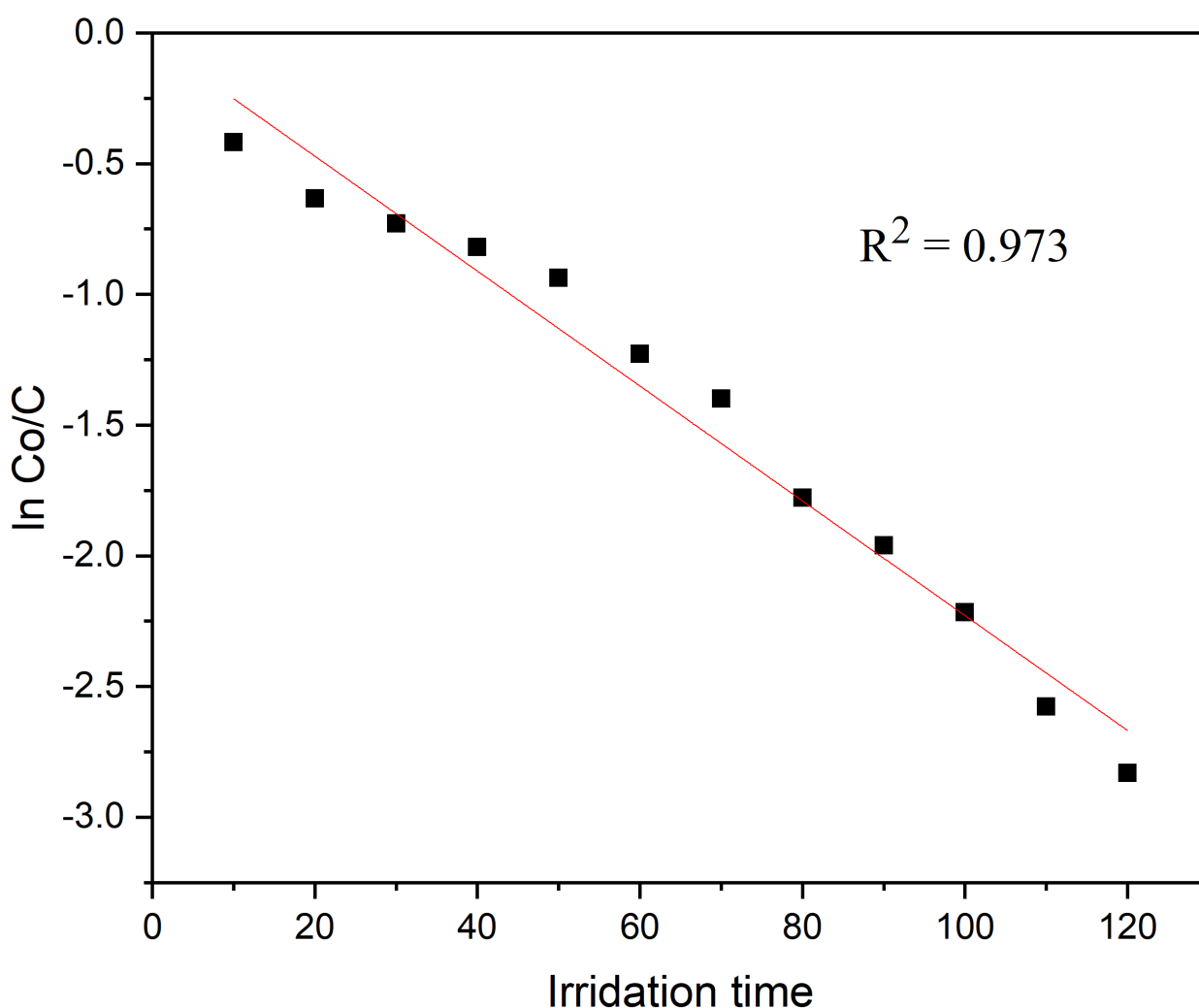


**Figure 7.** Kinetic rate constant for the degradation of CR dye.

### 3. Photo-Catalytic Mechanism

The electron-hole pairs' effective separation and efficient ultraviolet light absorption are two potential mechanisms for enhancing the photo-catalytic performance of the POA/g-$C_3N_4$/ZnO photo-catalyst. In Figure 8, a potential photo-catalytic system of POA/g-$C_3N_4$/ZnO has been presented for the degradation of CR. ZnO and POA can be excited when exposed to UV light because of their intermediate bandgap energies of 3.37 eV and 2.46 eV, respectively. Owing to the higher negative conduction band (CB) of POA ($-1.15$ eV) than that of ZnO ($+0.43$ eV), the photo-induced electron of POA can transfer to the conduction band (CB) of ZnO [39]. $O_2$ could be converted to $H_2O_2$ ($+0.674$ eV) by the electrons in the CB of the ZnO, and $H_2O_2$ could then interact with electrons to form

$OH^{\bullet}$. While g-$C_3N_4$ is an electron acceptor, some ZnO electrons may also be transported to g-$C_3N_4$ to produce $O_2^{\bullet-}$. In the breakdown of CR, both $O_2^{\bullet-}$ and $OH^{\bullet}$ participate [40]. On the other hand, the generation of $h^+$ in ZnO was carried to the valence band of POA and interacted with CR to produce $CO_2$, $H_2O$, or other intermediate products. The ZnO, g-$C_3N_4$, and POA synergistic interaction in ternary systems improves the separation efficiency of $e^-/h^+$, leading to significantly better CR degradation performance [41].
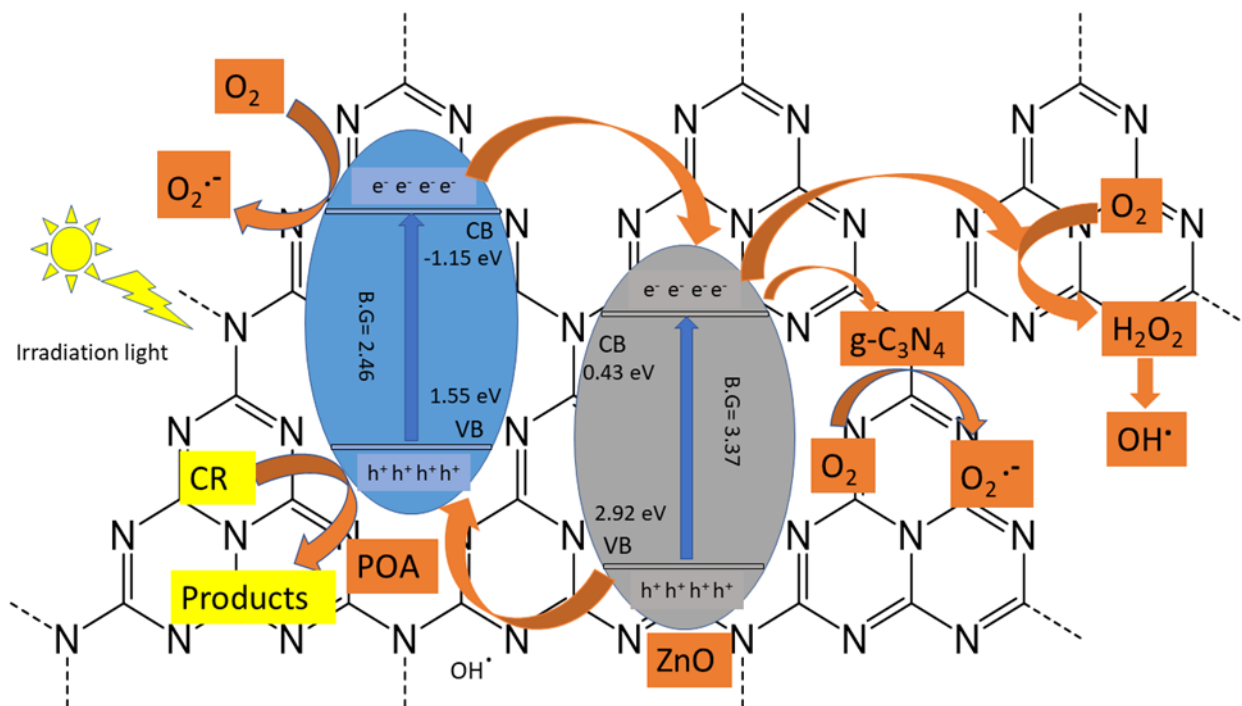


**Figure 8.** The suggested photo-reaction pathway of POA/g-$C_3N_4$/ZnO photo-catalyst composite for the CR dye degradation under UV light.

## 4. Experimental Section

### 4.1. Materials

Urea ($CH_4N_2O$, 99%), zinc nitrate (Zn $(NO_3)_2 \cdot 6H_2O$, 99%), and ethanol ($C_2H_6O$, 95%), sodium hydroxide (NaOH, 97%) Hydrochloric acid (HCl, 99%), *o*-anisidine monomer ($CH_3OC_6H_4NH_2$, 99.5%), nitric acid ($HNO_3$, 98%), ammonium persulfate (($NH_4)_2S_2O_8$) and 4,4′-diaminodiphenylamine sulfate hydrate ($C_{12}H_{15}N_3O_4S$, 99%) were purchased from Aladdin Reagent Co., Ltd. (Shanghai, China), and Congo red ($C_{32}H_{22}N_6Na_2O_6S_2$, 89%) dye was purchased from Tianjin Tianhe Chemical Reagent Factory (Tianjin China). The whole experiment proceeded with deionized (DI) water ($H_2O$). All of the chemicals and reagents are analytically pure and used without any purification.

### 4.2. Synthesis of g-$C_3N_4$

The direct decomposition method was used to synthesize the g-$C_3N_4$. First, we filled the silica crucible with 100 g of analytical-grade $CH_4N_2O$ and covered it with a lid. Then we placed the crucible in a muffle furnace and allowed it to heat for 2 h. Finally, the required g-$C_3N_4$ was washed with $C_2H_6O$ and DI $H_2O$ to remove the impurities [42].

### 4.3. Synthesis of ZnO NPs

The co-precipitation method was used to synthesize the ZnO NPs. First, 1 M aqueous solution of Zn $(NO_3)_2 \cdot 6H_2O$ was prepared and stirred for 30 min. Then, a 1 M aqueous solution of NaOH was prepared. The synthesized NaOH solution was added dropwise in Zn $(NO_3)_2 \cdot 6H_2O$ solution with high-speed stirring for 60 min. The reaction was allowed to

proceed for 150 min. After that, the white precipitate was allowed to settle down overnight. The prepared solution was separated carefully by centrifugation. Finally, the ZnO NPs precipitates were cleaned with DI $H_2O$ and $C_2H_6O$, and dried in an electrical oven at about 120 °C [43].

### 4.4. Regeneration of ZnO NPs

The previously obtained ZnO NPs were modified by treating them with 0.1 M $HNO_3$. An amount of 5 g of ZnO NPs was added to 10 mL of $HNO_3$ solution and stirred for 12 h. Then it was sonicated for 2 h. Afterward, it was centrifuged and dried in an oven at 80 °C for half an hour.

### 4.5. Synthesis of POA/g-C₃N₄/ZnO Composites

A facile in-situ chemical oxidative polymerization technique was employed to synthesize the POA/g-$C_3N_4$/ZnO composites. For sample 1 (S1), 0.08 g of g-$C_3N_4$ was added to 20 mL of 2 M HCl solution and stirred for 24 h. Afterward, 1 g of regenerated ZnO NPs was added and stirred for 1 h. Next, 1 mL of $CH_3OC_6H_4NH_2$ was added dropwise into the above-prepared g-$C_3N_4$/ZnO solution and stirred for another half an hour. For polymerization, $(NH_4)_2S_2O_8$ (0.1 M) was added to the solution. Moreover, $C_{32}H_{22}N_6Na_2O_6S_2$ was added as an initiator to increase the reaction rate. The precipitate was formed and stirred for 24 h. Finally, the solution was centrifuged and dried at 70 °C. Similarly, the same procedure was used for the synthesis of sample 2 (S2) and sample 3 (S3); in S2 2 mL $CH_3OC_6H_4NH_2$ was used, and for S3 3 mL $CH_3OC_6H_4NH_2$ was used [44].

### 4.6. Test of Photo-Catalytic Activity

ZnO NPs, g-$C_3N_4$, and POA/g-$C_3N_4$/ZnO composites were evaluated under UV light for the degradation of CR. In the first experiment, 0.1 g of ZnO NPs was added into a 100-ppm solution of CR to determine the photo-catalytic performance of the material. In the second experiment, 0.1 g of g-$C_3N_4$ was added into a 100-ppm solution of CR to determine the photo-catalytic performance of the material. The same procedure was followed to evaluate the performance of synthesized POA/g-$C_3N_4$/ZnO composites. The solution was placed in the dark for 1 h to attain the adsorption–desorption equilibrium before illuminating the UV light. The experiment was performed for 120 min, in which the absorbance of the sample was evaluated at 10 min intervals using UV-visible spectroscopy (Lambda 25, Perkin Elmer Shanghai, China) at 497 nm. The sample was centrifuged at 4500 rpm for each measurement to separate the liquid pollutant from the powder catalyst. The photo-catalytic degradation efficiency (*E*) was obtained by the following formula as shown in Equation (3):

$$E = \left(1 - \frac{C}{C_0}\right) \times 100\% \; OR \; \left(1 - \frac{A}{A_0}\right) \times 100\% \tag{3}$$

*C* is the CR concentration at different times, and $C_0$ is the initial concentration at CR adsorption equilibrium, and *A* and $A_0$ are the corresponding absorption values.

## 5. Conclusions

In summary, poly(*o*-anisidine)/graphitic carbon nitride/zinc oxide composites were synthesized by a facile in situ chemical oxidative polymerization method. The synthesized POA/g-$C_3N_4$/ZnO composite was tested as an active photo-catalyst for the Congo red (CR) degradation under UV light. The photo-catalytic activity of the synthesized POA/g-$C_3N_4$/ZnO composites was higher than the pristine g-$C_3N_4$ and ZnO. The result revealed that g-$C_3N_4$, ZnO, and POA are suitable to alter the bandgap energy and enhance the $e^-$/$h^+$ pairs recombination rate, which facilitates the higher decomposition of CR molecules by POA/g-$C_3N_4$/ZnO under the UV light. Overall, the synthesis and photo-catalytic activity of POA/g-$C_3N_4$/ZnO composites for degrading CR dyes were non-toxic, economical, and environmentally friendly.

## References

1. Li, C.; Wu, X.; Shan, J.; Liu, J.; Huang, X. Preparation, Characterization of Graphitic Carbon Nitride Photo-Catalytic Nanocomposites and Their Application in Wastewater Remediation: A Review. *Crystals* **2021**, *11*, 723. [CrossRef]
2. Zarei, M.; Bahrami, J.; Zarei, M. Zirconia nanoparticle-modified graphitic carbon nitride nanosheets for effective photocatalytic degradation of 4-nitrophenol in water. *Appl. Water Sci.* **2019**, *9*, 175. [CrossRef]
3. Buthelezi, S.P.; Olaniran, A.O.; Pillay, B. Textile dye removal from wastewater effluents using bioflocculants produced by indigenous bacterial isolates. *Molecules* **2012**, *17*, 14260–14274. [CrossRef] [PubMed]
4. Doornbusch, G.; van der Wal, M.; Tedesco, M.; Post, J.; Nijmeijer, K.; Borneman, Z. Multistage electrodialysis for desalination of natural seawater. *Desalination* **2021**, *505*, 114973. [CrossRef]
5. Saleh, I.A.; Zouari, N.; Al-Ghouti, M.A. Removal of pesticides from water and wastewater: Chemical, physical and biological treatment approaches. *Environ. Technol. Innov.* **2020**, *19*, 101026. [CrossRef]
6. Van Tran, V.; Park, D.; Lee, Y.-C. Hydrogel applications for adsorption of contaminants in water and wastewater treatment. *Environ. Sci. Pollut. Res.* **2018**, *25*, 24569–24599. [CrossRef]
7. Zuo, K.; Wang, K.; DuChanois, R.M.; Fang, Q.; Deemer, E.M.; Huang, X.; Xin, R.; Said, I.A.; He, Z.; Feng, Y. Selective membranes in water and wastewater treatment: Role of advanced materials. *Mater. Today* **2021**, *50*, 516–532. [CrossRef]
8. Kumar, A.; Nidheesh, P.; Kumar, M.S. Composite wastewater treatment by aerated electrocoagulation and modified peroxi-coagulation processes. *Chemosphere* **2018**, *205*, 587–593. [CrossRef]
9. Ejraei, A.; Aroon, M.A.; Saravani, A.Z. Wastewater treatment using a hybrid system combining adsorption, photocatalytic degradation and membrane filtration processes. *J. Water Process Eng.* **2019**, *28*, 45–53. [CrossRef]
10. Wang, A.; Wang, Y.; Yu, W.; Huang, Z.; Fang, Y.; Long, L.; Song, Y.; Cifuentes, M.P.; Humphrey, M.G.; Zhang, L. $TiO_2$–multi-walled carbon nanotube nanocomposites: Hydrothermal synthesis and temporally-dependent optical properties. *RSC Adv.* **2016**, *6*, 20120–20127. [CrossRef]
11. Manea, Y.K.; Khan, A.M.; Nabi, S.A. Facile synthesis of Mesoporous Sm@ POA/TP and POA/TP nanocomposites with excellent performance for the photocatalytic degradation of MB and MG dyes. *J. Alloys Compd.* **2019**, *791*, 1046–1062. [CrossRef]
12. Khamngoen, K.; Paradee, N.; Sirivat, A. Chemical oxidation polymerization and characterization of poly ortho-anisidine nanoparticles. *J. Polym. Res.* **2016**, *23*, 172. [CrossRef]
13. Xu, B.; Ahmed, M.B.; Zhou, J.L.; Altaee, A.; Xu, G.; Wu, M. Graphitic carbon nitride based nanocomposites for the photocatalysis of organic contaminants under visible irradiation: Progress, limitations and future directions. *Sci. Total Environ.* **2018**, *633*, 546–559. [CrossRef] [PubMed]
14. Palanivel, B.; Mani, A. Conversion of a type-II to a Z-scheme heterojunction by intercalation of a 0D electron mediator between the integrative $NiFe_2O_4$/g-$C_3N_4$ composite nanoparticles: Boosting the radical production for photo-fenton degradation. *ACS Omega* **2020**, *5*, 19747–19759. [CrossRef]
15. Ong, W.-J.; Tan, L.-L.; Ng, Y.H.; Yong, S.-T.; Chai, S.-P. Graphitic carbon nitride (g-$C_3N_4$)-based photocatalysts for artificial photosynthesis and environmental remediation: Are we a step closer to achieving sustainability? *Chem. Rev.* **2016**, *116*, 7159–7329. [CrossRef]
16. Vinothkumar, V.; Kesavan, G.; Chen, S.-M. Graphitic carbon nitride nanosheets incorporated with polypyrrole nanocomposite: A sensitive metal-free electrocatalyst for determination of antibiotic drug nitrofurantoin. *Colloids Surf. A Physicochem. Eng. Asp.* **2021**, *629*, 127433. [CrossRef]
17. Paul, D.R.; Gautam, S.; Panchal, P.; Nehra, S.P.; Choudhary, P.; Sharma, A. ZnO-modified g-$C_3N_4$: A potential photocatalyst for environmental application. *ACS Omega* **2020**, *5*, 3828–3838. [CrossRef]
18. Moafi, H.F.; Zanjanchi, M.A.; Shojaie, A.F. Tungsten-doped ZnO nanocomposite: Synthesis, characterization, and highly active photocatalyst toward dye photodegradation. *Mater. Chem. Phys.* **2013**, *139*, 856–864. [CrossRef]

19. Fang, J.; Fan, H.; Ma, Y.; Wang, Z.; Chang, Q. Surface defects control for ZnO nanorods synthesized by quenching and their anti-recombination in photocatalysis. *Appl. Surf. Sci.* **2015**, *332*, 47–54. [CrossRef]

20. Saravanan, R.; Agarwal, S.; Gupta, V.K.; Khan, M.M.; Gracia, F.; Mosquera, E.; Narayanan, V.; Stephen, A. Line defect $Ce^{3+}$ induced $Ag/CeO_2/ZnO$ nanostructure for visible-light photocatalytic activity. *J. Photochem. Photobiol. A Chem.* **2018**, *353*, 499–506. [CrossRef]

21. Yim, K.; Lee, J.; Lee, D.; Lee, M.; Cho, E.; Lee, H.S.; Nahm, H.-H.; Han, S. Property database for single-element doping in ZnO obtained by automated first-principles calculations. *Sci. Rep.* **2017**, *7*, 40907. [CrossRef] [PubMed]

22. Mohd, S.; Wani, A.A.; Khan, A.M. ZnO/POA functionalized metal-organic framework ZIF-8 nanomaterial for dye removal. *Clean. Chem. Eng.* **2022**, *3*, 100047. [CrossRef]

23. Nie, Y.-C.; Yu, F.; Wang, L.-C.; Xing, Q.-J.; Liu, X.; Pei, Y.; Zou, J.-P.; Dai, W.-L.; Li, Y.; Suib, S.L. Photocatalytic degradation of organic pollutants coupled with simultaneous photocatalytic $H_2$ evolution over graphene quantum dots/Mn-N-$TiO_2$/g-$C_3N_4$ composite catalysts: Performance and mechanism. *Appl. Catal. B Environ.* **2018**, *227*, 312–321. [CrossRef]

24. Liu, W.; Wang, M.; Xu, C.; Chen, S. Facile synthesis of g-$C_3N_4$/ZnO composite with enhanced visible light photooxidation and photoreduction properties. *Chem. Eng. J.* **2012**, *209*, 386–393. [CrossRef]

25. Deng, Y.; Liu, J.; Huang, Y.; Ma, M.; Liu, K.; Dou, X.; Wang, Z.; Qu, S.; Wang, Z. Engineering the photocatalytic behaviors of g/$C_3N_4$-based metal-free materials for degradation of a representative antibiotic. *Adv. Funct. Mater.* **2020**, *30*, 2002353. [CrossRef]

26. Ahmad, I. Comparative study of metal (Al, Mg, Ni, Cu and Ag) doped ZnO/g-$C_3N_4$ composites: Efficient photocatalysts for the degradation of organic pollutants. *Sep. Purif. Technol.* **2020**, *251*, 117372. [CrossRef]

27. Wu, H.; Lin, S.; Chen, C.; Liang, W.; Liu, X.; Yang, H. A new ZnO/rGO/polyaniline ternary nanocomposite as photocatalyst with improved photocatalytic activity. *Mater. Res. Bull.* **2016**, *83*, 434–441. [CrossRef]

28. Li, X.; Wang, B.; Yin, W.; Di, J.; Xia, J.; Zhu, W.; Li, H. $Cu^{2+}$ modified g-$C_3N_4$ photocatalysts for visible light photocatalytic properties. *Acta Phys.-Chim. Sin.* **2020**, *36*, 1902001. [CrossRef]

29. Pandiselvi, K.; Fang, H.; Huang, X.; Wang, J.; Xu, X.; Li, T. Constructing a novel carbon nitride/polyaniline/ZnO ternary heterostructure with enhanced photocatalytic performance using exfoliated carbon nitride nanosheets as supports. *J. Hazard. Mater.* **2016**, *314*, 67–77. [CrossRef]

30. Wan, Z.; Zhang, G.; Wu, X.; Yin, S. Novel visible-light-driven Z-scheme Bi12GeO20/g-$C_3N_4$ photocatalyst: Oxygen-induced pathway of organic pollutants degradation and proton assisted electron transfer mechanism of Cr (VI) reduction. *Appl. Catal. B Environ.* **2017**, *207*, 17–26. [CrossRef]

31. Thi, T.A.N.; Vu, A.-T. Nanocomposite ZnO/g-$C_3N_4$ for Improved Degradation of Dyes under Visible Light: Facile Preparation, Characterization, and Performance Investigations. *Bull. Chem. React. Eng. Catal.* **2022**, *17*, 403–419.

32. Saravanan, R.; Khan, M.M.; Gupta, V.K.; Mosquera, E.; Gracia, F.; Narayanan, V.; Stephen, A. ZnO/Ag/CdO nanocomposite for visible light-induced photocatalytic degradation of industrial textile effluents. *J. Colloid Interface Sci.* **2015**, *452*, 126–133. [CrossRef] [PubMed]

33. Yan, M.; Zhu, F.; Gu, W.; Sun, L.; Shi, W.; Hua, Y. Construction of nitrogen-doped graphene quantum dots-BiVO4/gC3N4 Z-scheme photocatalyst and enhanced photocatalytic degradation of antibiotics under visible light. *RSC Adv.* **2016**, *6*, 61162–61174. [CrossRef]

34. Singh, J.; Kalamdhad, A.S.; Koduru, J.R. Potential degradation of hazardous dye Congo red by nano-metallic particles synthesized from the automobile shredder residue. *Nanotechnol. Environ. Eng.* **2017**, *2*, 10. [CrossRef]

35. Sowmya, S.; Madhu, G.; Hashir, M. Studies on Nano-Engineered $TiO_2$ Photo Catalyst for Effective Degradation of Dye. *IOP Conf. Ser. Mater. Sci. Eng.* **2018**, *310*, 012026. [CrossRef]

36. Khairnar, S.D.; Patil, M.R.; Shrivastava, V.S. Hydrothermally synthesized nanocrystalline $Nb_2O_5$ and its visible-light photocatalytic activity for the degradation of congo red and methylene blue. *Iran. J. Catal.* **2018**, *8*, 143–150.

37. Sun, J.-H.; Wang, Y.-K.; Sun, R.-X.; Dong, S.-Y. Photodegradation of azo dye Congo Red from aqueous solution by the $WO_3$–$TiO_2$/activated carbon (AC) photocatalyst under the UV irradiation. *Mater. Chem. Phys.* **2009**, *115*, 303–308. [CrossRef]

38. Villarreal, R.; Luque-Morales, M.; Chinchillas-Chinchillas, M.; Luque, P. Langmuir-Hinshelwood-Hougen-Watson model for the study of photodegradation properties of zinc oxide semiconductor nanoparticles synthetized by Peumus boldus. *Results Phys.* **2022**, *36*, 105421. [CrossRef]

39. Hanumaiah Anupama, B.; AL-Gunaid, M.Q.; Shivanna Shasikala, B.; Theranya Ereppa, S.; Kavya, R.; Hatna Siddaramaiah, B.; Sangameshwara Madhukar, B. Poly (o-anisidine) Encapsulated $K_2ZrO_3$ Nano-core based Gelatin Nano Composites: Investigations of Optical, Thermal, Microcrystalline and Morphological Characteristics. *ChemistrySelect* **2022**, *7*, e202201621. [CrossRef]

40. Faisal, M.; Rashed, M.A.; Ahmed, J.; Alsaiari, M.; Jalalah, M.; Alsareii, S.; Harraz, F.A. Au nanoparticles decorated polypyrrole-carbon black/g-$C_3N_4$ nanocomposite as ultrafast and efficient visible light photocatalyst. *Chemosphere* **2022**, *287*, 131984. [CrossRef]

41. Thomas, M.; Naikoo, G.A.; Sheikh, M.U.D.; Bano, M.; Khan, F. Effective photocatalytic degradation of Congo red dye using alginate/carboxymethyl cellulose/$TiO_2$ nanocomposite hydrogel under direct sunlight irradiation. *J. Photochem. Photobiol. A Chem.* **2016**, *327*, 33–43. [CrossRef]

42. Yao, S.; Xue, S.; Peng, S.; Jing, M.; Qian, X.; Shen, X.; Li, T.; Wang, Y. Synthesis of graphitic carbon nitride at different thermal-pyrolysis temperature of urea and it application in lithium–sulfur batteries. *J. Mater. Sci. Mater. Electron.* **2018**, *29*, 17921–17930. [CrossRef]

43. Ghorbani, H.R.; Mehr, F.P.; Pazoki, H.; Rahmani, B.M. Synthesis of ZnO nanoparticles by precipitation method. *Orient. J. Chem* **2015**, *31*, 1219–1221. [CrossRef]

44. Alenizi, M.; Kumar, R.; Aslam, M.; Alseroury, F.; Barakat, M. Construction of a ternary gC$_3$N$_4$/TiO$_2$@ polyaniline nanocomposite for the enhanced photocatalytic activity under solar light. *Sci. Rep.* **2019**, *9*, 12091. [CrossRef] [PubMed]